Original Article
Preparation and evaluation of a ^{68}Ga-labeled RGD-containing octapeptide for noninvasive imaging of angiogenesis: biodistribution in non-human primate

Irina Velikyan[1], Örjan Lindhe[2]

[1]Section of Nuclear Medicine and PET, Department of Surgical Sciences, Uppsala University, Uppsala, Sweden;
[2]Uppsala Imanet, GE Healthcare, SE-75109, Uppsala, Sweden

Abstract: Monitoring general disease marker such as angiogenesis may contribute to the development of personalized medicine and improve therapy outcome. Readily availability of positron emitter based imaging agents providing quantification would expand clinical positron emission tomography (PET) applications. Generator produced ^{68}Ga provides PET images of high resolution and the half-life time frame is compatible with the pharmacokinetics of small peptides comprising arginine-glycine-aspartic acid (RGD) sequence specific to $\alpha_v\beta_3$ integrin receptors. The main objective of this study was to develop a method for ^{68}Ga-labeling of RGD containing bicyclic octapeptide ([^{68}Ga]Ga-DOTA-RGD) with high specific radioactivity and preclinically assess its imaging potential. DOTA-RGD was labeled using generator eluate preconcentration technique and microwave heating. The binding and organ distribution properties of [^{68}Ga]Ga-DOTA-RGD were tested in vitro by autoradiography of frozen tumor sections, and in vivo in mice carrying a Lewis Lung carcinoma graft (LL2), and in non-human primate (NHP). Another peptide with aspartic acid-glycine-phenylalanine sequence was used as a negative control. The full ^{68}Ga radioactivity eluted from two generators was quantitatively incorporated into 3-8 nanomoles of the peptide conjugates. The target binding specificity was confirmed by blocking experiments. The specific uptake in the LL2 mice model was observed in vivo and confirmed in the corresponding ex vivo biodistribution experiments. Increased accumulation of the radioactivity was detected in the wall of the uterus of the female NHP probably indicating neovascularization. [^{68}Ga]Ga-DOTA-RGD demonstrated potential for the imaging of angiogenesis.

Keywords: [68]Ga, RGD, PET, animal PET, angiogenesis, cancer, endometriosis, Lewis lung carcinoma, organ distribution, frozen section autoradiography, whole body autoradiography

Introduction

The process of new capillary growth known as angiogenesis is involved in physiological processes such as repair of wounds, placenta formation, and female reproductive cycle [1]. Pathophysiological processes can be caused either by excessive or insufficient angiogenesis. The upregulated angiogenesis contributes to cancer, blinding diseases, psoriasis, arthritis, endometriosis, multiple sclerosis, obesity etc. Considerable number of antiangiogenic drugs, particularly for cancer treatment has been developed. Monitoring of angiogenic activity would allow validation of antiangiogenic drug efficacy on early stage and on personalized basis in terms of treatment selection as well as monitoring angiogenesis activity and

thus response to the treatment. Sensitive, quantitative, and whole body imaging methods, e.g. positron emission tomography (PET) have potential to assist antiangiogenetic drug development based on microdosing concept [2, 3].

Molecular targets such as integrin receptors, vascular endothelial growth factor (VEGF) receptors, and matrix metalloproteinases 9 (MMP-9) have been identified and the respective imaging agents have been developed [4]. The most intensive research has been conducted in targeting integrin receptors and developing peptides that could mimic cell adhesion proteins and bind to the receptors [5].

An extensive number of peptide ligands with an exposed arginine-glycine-aspartic acid (RGD)

sequence for binding to $\alpha_v\beta_3$ integrin receptors has been developed for the imaging with such modalities as PET, single photon emission computed tomography (SPECT), optical, magnetic resonance (MR), and ultrasound during the last two decades [5, 6]. The influence of the major components of the agent structure such as chelator moiety (DOTA, NOTA, DTPA, TETA, TE2A, TRAP-Pr, NOPO, protoporphyrinIX, macrobicyclic), pharmacokinetic modifiers (polyethylene glycol, hydrophilic amino acids, sugar), and multivalency of RGD motif on the affinity and pharmacokinetics has been studied preclinically in mice with various cancer xenografts or ischemic or atherosclerotic models [7-28]. The enhancement of the valency from mono- to di- to tetrameric cyclic RGD commonly results in increased uptake, though the mechanism is unclear [29-32]. However, further optimization is required in order to find fine balance between the tumor uptake on the one hand and blood clearance and kidney accumulation on the other hand.

RGD analogues have been labeled with halogen radionuclides such as [18]F [9, 33-36] and [125]I [10], metal radionuclides such as [99m]Tc [37, 38], [64]Cu [17, 39], [111]In [14], [89]Zr [40] and [68]Ga [14, 15, 17, 35, 41] and pre-clinically evaluated for the imaging with SPECT and PET [42]. Clinical trials have been conducted using [18F]Galacto-RGD [43-47], [18F]-AH111585 [48, 49], and [99mTc]-NC100692, [99mTc]-RGD-SC-RGD-SY [37, 50, 51] imaging agents. The correlation between the tracer uptake and $\alpha_v\beta_3$ expression on endothelial cells was proven. ^{99m}Tc-labeled analogues were used for the imaging of malignant melanoma [50] and breast cancer [51] demonstrating high detection rate (86%) and no adverse effects were observed. However, PET offers intrinsic advantages over SPECT in higher sensitivity, throughput, and quantification. [18F]Galacto-RGD/PET used in patients affected by squamous cell carcinoma of the head and neck (SCCHN), breast, melanoma, colon cancer demonstrated low radiation dose, high metabolic stability, safety, and potential for planning and monitoring of the treatment [43, 52]. However, the uptake in the urinary track and bladder could precluding diagnostic imaging in those areas. Another agent, [18F]AH111585, assessed in patients with metastatic breast cancer for the safety, stability, and tumor kinetics investigation [49], demonstrated net-irreversible uptake and higher image

contrast presenting advantage over [18F]Galacto-RGD. ^{68}Ga-labeled agent, [^{68}Ga]-NOTA-RGD, demontrated acceptable effective radiation dose in oncological patients [53].

The development of molecular imaging in the direction of personalized medicine for higher therapeutic efficiency requires also the ready availability of corresponding imaging agents with sufficiently high specific radioactivity (SRA) crucial for the accurate quantification of PET examination. Positron emitting ^{68}Ga provides a number of advantages. It is produced from a long shelf-life generator (1-2 years) allowing PET studies without on-site cyclotrons. It's nuclear properties (89% β^+) provide high quality images. The half-life of 68 min matches the pharmacokinetic time window of the most of small peptides. Straightforward and simple labeling chemistry make this radionuclide a very potential and attractive tool for the clinical nuclear medicine. The use of ^{68}Ga could also enable PET clinical examinations at medical centers remote from cyclotrons and radiotracer distribution sources. A method for the fast labeling with high SRA has been developed previously [13]. Thus, implementation of ^{68}Ga based RGD imaging agents may provide the advantage of easy accessability of the latter as well as benefits of PET such as high sensitivity, specificity, accuracy, high detection rate and above all quantification possibility that may considerably contribute to the development of individualized medicine.

This study was set up to develop a labeling protocol for the preparation of [^{68}Ga]Ga-DOTA-RGD of high SRA, and to evaluate the resulting agent *in vitro* and *in vivo*, particularly, to perform biodistribution in non-human primate (NHP) in order to investigate the relevance of this candidate for angiogenesis imaging.

Material and methods

Materials

DOTA-RGD (RGD = Cys2-6; c[CH$_2$CO-Lys(DOTA)-Cys-Arg-Gly-Asp-Cys-Phe-Cys]-CCPEG-NH$_2$), DOTA-DGF (DGF = Cys2-6; c[CH$_2$CO-Lys(DOTA)-Cys-Gly-Asp-Phe-Cys-Arg-Cys]-CCPEG-NH$_2$), and NC100717 (Cys2-6; c[CH$_2$CO-Lys(DOTA)-Cys-Arg-Gly-Asp-Cys-Phe-Cys]-CCPEG-NH$_2$) were received from Amersham Health (Department of Synthetic Chemistry, Amersham Health, Olso, Norway) [54]. HEPES (4-(2-Hydroxyethyl)

piperazine-1-ethanesulfonic acid) and double distilled hydrochloric acid (Riedel de Haën) were obtained from Sigma-Aldrich Sweden (Stockholm, Sweden). Sodium dihydrogen phosphate, disodium hydrogen phosphate and trifluoroacetic acid (TFA) were obtained from Merck (Darmstadt, Germany). The purchased chemicals were used without further purification. Deionized water (18.2 MΩ), produced with a Purelab Maxima Elga system (Bucks, UK) was used in all reactions.

Radiochemistry

^{68}Ga production and processing: ^{68}Ga ($t_{1/2}$ = 68 min, β^+ = 89% and EC = 11%) was available from a ^{68}Ge/^{68}Ga-generator-system (Cyclotron Co., Ltd, Obninsk, Russia) where the ^{68}Ge ($t_{1/2}$ = 270.8 d) was attached to a column of an inorganic matrix based on titanium dioxide. The nominal ^{68}Ge activity loaded onto the generator column was 1850 MBq (50 mCi). The specified shelf-life of the generator was 2-3 years. The ^{68}Ga was eluted with 6 mL of 0.1 M hydrochloric acid.

The ^{68}Ge/^{68}Ga-generator was eluted according to the manufacturer protocol with 6 mL 0.1 M solution. Five mL of 30% HCl was added to the 6 mL of the generator eluate giving finally a HCl concentration of 4.0 M. The resulting 11 mL solution in total was passed through an anion exchange column at a flow rate of 4 mL/min (linear flow speed 25 cm/min) at room temperature [13]. The ^{68}Ga was then eluted with small fractions of deionized water (50-200 µl) at a flow rate of 0.5 mL/min. The pre-concentration has successfully been performed for the eluates (12 mL) of two generators, increasing the amount of radioactivity and prolonging the shelf-life of the generators [55].

^{68}Ga-labeling of DOTA-RGD and DOTA-DGF: The pH of the pre-concentrated/purified ^{68}Ge/^{68}Ga-generator eluates (2×6 mL) was adjusted to pH~4.6 by adding sodium hydroxide and HEPES to give finally a 1.5 M solution with regard to HEPES. Then 3-8 nanomols of the peptide conjugates dissolved in deionized water (0.1 mM) were added. The reaction mixture was transferred to a Pyrex glass vial with an insert to accommodate the small volume (200 ± 20 µL) for microwave heating. The heating time in the microwave oven was 1 min at 95 ± 5°C. The microwave heating was performed in a Smith-

Creator™ monomodal microwave cavity producing continuous irradiation at 2450 MHz (Biotage, Uppsala, Sweden). The temperature, pressure and irradiation power were monitored during the course of the reaction. The reaction vial was cooled down with pressurized air after completed irradiation. The obtained product was analyzed by UV-radio-HPLC using reverse phase separation mechanism.

HPLC and LC-ESI-MS analysis: Analytical liquid chromatography (LC) was performed using a HPLC system from Beckman (Fullerton, CA, USA) consisting of a 126 pump, a 166 UV detector and a radiation flow detector (Bioscan) coupled in series. Data acquisition and handling were performed using the Beckman System Gold Nouveau Chromatography Software Package. The column used was a Vydac RP 300 Å HPLC column (Vydac, USA) with the dimensions 150 mm×4.6 mm, 5 µm particle size. The gradient elution was applied with the following parameters: A = 10 mM TFA; B = 70% acetonitrile (MeCN), 30% H_2O, 10 mM TFA with UV-detection at 220 nm; flow was 1.2 mL/min; 0-2 min isocratic 20% B, 20-90% B linear gradient 8 min, 90-20% B linear gradient 2 min.

Liquid chromatography electrospray ionization mass spectrometry (LC-ESI-MS) was performed using a Fisons Platform (Micromass, Manchester, UK) with positive mode scanning and detecting $[M+2H]^{2+}$ and $[M+3H]^{3+}$ species. DOTA-RGD at m/z = 549.1 for $[M+2H]^{2+}$ and 823.44 for $[M+3H]^{3+}$ and ^{69,71}Ga-DOTA-DGF at m/z = 857 for $[M+2H]^{2+}$ and 571 for $[M+3H]^{3+}$. The ^{69,71}Ga-conjugate synthesised under indentical to labeling conditions was used for the identification of the radio-HPLC chromatogram signals.

Biological evaluation

All animals were handled according to the guidelines by the Swedish Animal Welfare Agency, and the experiments were approved by the local Ethics Committee for Animal Research, permit no: C46/3.

Lewis lung carcinoma mouse model: The *in vivo* studies were carried out in adult female C57Bl/6J mice (28-33 g) (Möllegård, Denmark) with s.c. tumor grafts. The mice were injected subcutaneously with tumor cells (approximately 1 million cells per tumor in 100 µl cell culture

medium) in the left hind leg. The tumors were allowed to grow for 14 days before the experiments were performed, and had then reached a weight of 0.61 ± 0.45 g (mean ± SD). The mouse Lewis Lung carcinoma cell line (LL2) (ATCC, CLR 1642, Rocksville, MD, USA) were cultured in Dulbecco's modified Eagle's medium with 4 mM L-glutamine adjusted to contain 1.5 g/L sodium bicarbonate and 4.5 g/L glucose, 10% fetal bovine serum, and PEST (penicillin 100 IU/ml and streptomycin 100 μg/ml). Cells were grown at 37°C in incubators with humidified air, equilibrated with 5% CO_2. The cells were trypsinized with trypsin-EDTA (0.25% trypsin, 0.02% EDTA in PBS without Ca and Mg), centrifuged and suspended in culture medium without serum to a concentration of 1×10^7 cells/ml.

In order to evaluate uptake in tumors and normal tissues, a biodistribution study was performed. Six mice with LL2 tumor grafts were injected intravenously with 100 μl [^{68}Ga]Ga-DOTA-RGD solution 3.3 ± 0.8 MBq (mean ± SD, approximately 0.14 nmol in PBS per animal), 60 min post injection the animals were sacrificed and organ were dissected out. For the assessment of the binding specificity three animals were co-injected with excess of NC-100717 (4 mg/kg). In addition to the tumor, blood, lung, liver, spleen, kidney, and muscle were collected, weighed and measured in an automated gamma counter. Organ values were calculated as standardized uptake value (SUV) and % of injected dose/g of tissue (%ID/g).

Frozen sections (20 μm) of the tumors were prepared in a cryomicrotome and put on superfrost glass slides. The slides were kept in a freezer (-20°C) until used. At the start of the experiment the slides were pre-incubated for 10 min in TRIS (50 mM, pH 7.4) buffer. The slides were then transferred to containers containing 10 nM [^{68}Ga]Ga-DOTA-RGD or 5 nM [^{68}Ga]Ga-DOTA-DGF in TRIS buffer. In a duplicate set of containers 15 and 5 nM of NC-100717 was added to block specific binding. After incubation for 60 min the slides were washed 3×3 min in buffer. The slides were dried at 37°C in an incubator for 10 min and together with the reference exposed to phosphor imager plates (Molecular Dynamics, Amersham Biosciences, UK) over night. The plates were scanned and the images were analyzed using ImageQuant TL software (GE Healthcare).

The mean values of the tissue regions of interest (ROIs) were corrected for background and expressed as average counts per pixel. Specific binding was defined as the difference between total binding and non-displaceable binding.

Two mice with LL2 tumor grafts were injected intravenously with 100 μl [^{68}Ga]Ga-DOTA-RGD solution 4.1 ± 0.1 MBq (mean ± SD, approx. 0.18 nmol in PBS per animal), one mouse was injected with 2.6 MBq [^{18}F]FDG. Sixty min post injection the animals were sacrificed and mounted in a gel of carboxy methylcellulose and water, frozen (-70°C) and subjected to tape section autoradiography according to Ullberg. Sagittal whole-body sections (60 μm) were collected onto tape (6890, 3M, USA) using a cryostat microtome (M-5160-C, PMV, Sweden) and dried. Radioluminograms were obtained by opposing tape sections to phosphor imaging plates (Molecular Dynamics, USA, purchased from Amersham Bioscience, Uppsala, Sweden). The plates were exposed > 120 min and scanned in a Phosphor Imager Model 400S (Molecular Dynamics, USA, purchased from Amersham Bioscience, Uppsala, Sweden).

For the dynamic scanning the mice were taken to the laboratory just before the experiment. After a short period of heating under a red-light bulb the animal was placed in a cylinder connected to an isoflurane vaporizer adjusted to deliver 2% isoflurane in a 55/45% mixture of oxygen and air. When the animal was unconscious a heparinized venous catheter was placed in a tail vein and connected to a 1 ml syringe with 0.9% NaCl and 10 IU heparin. The animal was subsequently placed on the scanner bed with its abdomen down and hind legs with tumors stretched out backward as much as possible from the body and covered with cloth to minimize heat loss. Heated air (< 40°C) was blown on the animal to reduce the loss of body temperature during the experiment. The tracer was injected as a bolus dose 30 seconds after the scanner start in a volume of 100 μl followed by 100 μl saline. After completion of the study the animals were decapitated under anaesthesia. Imaging of mice was performed on an animal PET R4 scanner (Concorde Microsystems, Inc.), with a computer-controlled bed and 10 cm transaxial and 8 cm axial field of view (FOV). All raw data were first sorted into 3-dimensional sinograms, followed by Fourier rebinning and 2-dimensional filtered back pro-

jection (2D-FBP) or iterative (OSEM) image reconstruction resulting in images with 2 mm resolution. Scatter correction, random counts and dead time correction were all incorporated into the reconstruction algorithm. Radiation attenuation in each animal was measured with a 10 minutes transmission scan using a spiraling point source containing [68]Ge/[68]Ga (18.5 MBq) before injection of the tracer. After the second emission study a 2 min emission scan was performed with the [68]Ge/^{68}Ga point source lying next to the left tumor in order to give a positive reference for the location of the tumor. The time frames for the emission acquisition were: 10×30 s, 5×60 s, and 10×120 s (duration 30 min, 21 frames). The acquisition time for the blank scan was 5 hours and the 600 seconds transmission scan was generated with an external rotating germanium-68 pin to correct the ensuing emission scan for attenuation scan. The amount of the injected activity was 3 MBq (approx. 0.14 nmol [^{68}Ga]Ga-DOTA-RGD in PBS per animal). Regions of interest (ROIs) were drawn on bladder, kidney, and tumor. Pharmacokinetic curves representing the radioactivity concentrations were calculated as activity in organ [кBq/mL].

Non-human primate: The NHP (Rhesus monkey, female) were sedated with ketamin (appr. 7 mg/kg) and transported to Uppsala Imanet AB. During transport the animal was monitored by pulse oximetry and supported by oxygen. The animal was weighed. One venous catheter was applied for tracer administration and one venous catheter for blood radioactivity and PK sampling. Propofol was administered until the animal was anesthetized enough to be intubated. After intubation the animal was maintained on sevoflurane inhalation anesthesia and artificial ventilation. The NHP anaesthesia was controlled by respirator at a sevoflurane concentration of about 3-8%. Tracrium inf. 0.3-0.6 mg/kg/h. A urine catheter (Nelaton, Silikon 2 v, 06 ch, 30 cm, 3 ml) will be put in the bladder for drainage. Ringer-Acetate (Fresenius-Kabi) 0, 5-1 ml/kg/h. Glucose 300 mg/ml was administered if necessary depending on the blood glucose state as measured. The blood loss was compensated with albumin 50 mg/ml in relation to the volume taken. Body temperature, heart rate, ECG, pCO_2, pO_2, SaO_2 and blood pressure were monitored throughout the PET study.

Imaging was performed on a Hamamatsu SHR 7700 PET scanner (Hamamatsu, Japan), with an aperture 30 cm, field of view 12 cm, and resolution 3.5 mm. Dynamic images were reconstructed in a of 2-dimensional filtered back projection (2D-FBP) 128×128 matrix with a pixel size of 4×4 mm using a 4 mm Hanning filter, scatter correction, random counts and dead time correction were all incorporated into the reconstruction algorithm. The time frames for the emission acquisition were: 2×60 s, 3×120 s, 4×180 s, 4×300 s, and 5×600 s (duration 90 min). The acquisition time for the blank scan was 12 hours and a 30 min transmission scan was generated with an external rotating germanium-68 pin to correct the ensuing emission scan for attenuation. The tracer was injected as a bolus dose followed by 1 ml saline. Blood samples (0.5 ml) for radioactivity measurements (0.5 ml) were taken at 1, 3, 6, 9, 12, 15, 30, 60, 90 minutes after RGD injection. Radioactivity was measured in plasma obtained after centrifugation. The amounts of the injected activity were 48 and 81 MBq [^{68}Ga]Ga-DOTA-RGD for the baseline and blocking study respectively. Regions of interest (ROIs) were drawn on the top of the uterus to be well clear of the bladder as well as in the middle of the bladder.

Imaging was performed on a GE Discovery ST[16] scanner (General Electric, USA), with a 15.7 cm axial and 60 cm transaxial field of view (FOV). Scatter correction, random counts and dead time correction were all incorporated into the reconstruction algorithm. Whole body PET examinations were performed with 240 s/bed. Radiation attenuation in each animal was measured with a full spiral 140 kV 80 mAs CT scan, section thickness 3.75 mm, Pitch 1.75:1, Speed 35. The amount of the injected radioactivity was 49 MBq for [^{68}Ga]Ga-DOTA-RGD and 104 MBq for [^{18}F]FDG. Whole body CT examination with venous phase of contrast media (20 ml Omnipaque, 240 mg/ml) was performed after the PET examination. The NHP anaesthesia and monitoring were controlled the same way as described in the Hammamatsu scanner protocol.

Results

Radiochemistry

The bicyclic octapeptides deriving from RGD-containing peptide NC-100717 [54], DOTA-RGD

A

Figure 1. Structural formulae of NC100717 (A), [^{68}Ga]Ga-DOTA-RGD (B) and [^{68}Ga]Ga-DOTA-DGF (C).

B

C
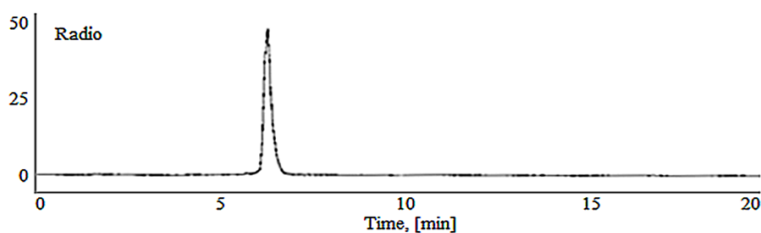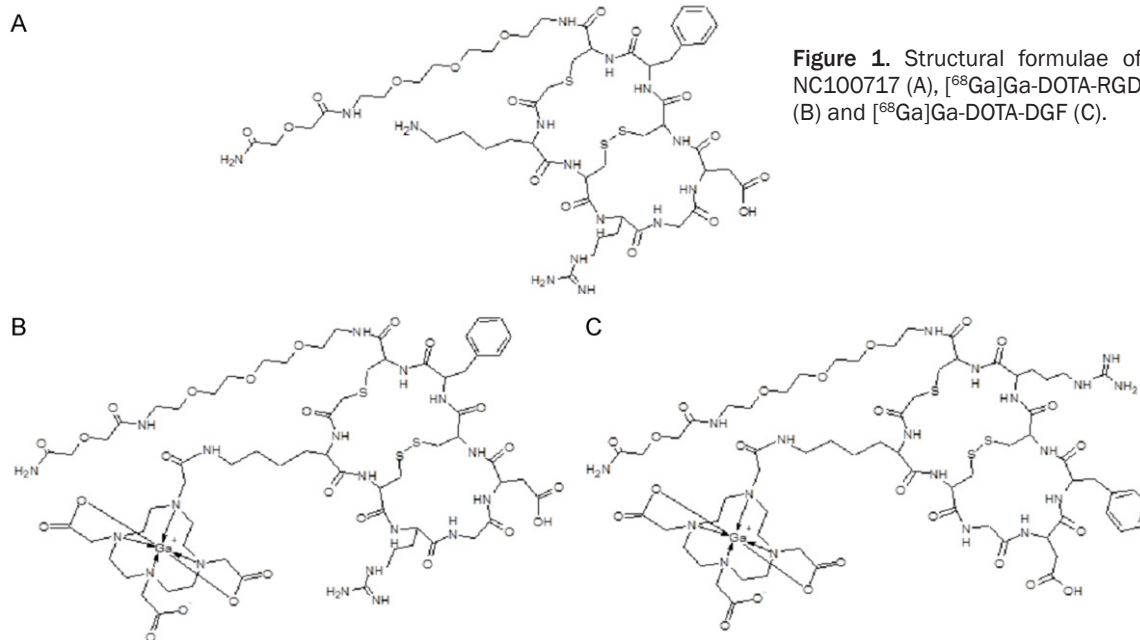
Figure 2. Radio-HPLC-radiochromatogram of a [^{68}Ga]Ga-DOTA-RGD preparation (4 nanomoles, 1 min microwave heating at 95 ± 5°C, total reaction volume 220 µL). The ^{68}Ga(III) incorporation was over 95%.

and DOTA-DGF, conjugated with a macrocyclic bifunctional chelator 1,4,7,10-tetraazacyclo-dodecane-1,4,7,10-tetraacetic acid (DOTA) at lysine residue were labeled with positron emitting radionuclide ^{68}Ga (**Figure 1**). The full ^{68}Ga radioactivity eluted from two generators was quantitatively (> 95%) incorporated into 3-8 nanomoles of the peptide conjugates. Further purification of the ^{68}Ga-labeled peptide conjugates was not required since the radionuclide incorporation was nearly quantitative with radiochemical purity over 95% and the buffer (HEPES) was compatible with the biological systems. The overall ^{68}Ga-labeling process was performed in 15-20 min starting from the end of the original generator elution thus resulting in non-decay corrected radiochemical yield of 83.8 ± 3.0%. SRA values, calculated with respect to the peptide amount, varied dependent on the generator age (152 ± 32 MBq/

nmol; range: 120-200 MBq/nmol) and the amount of the precursor (3-5 nanomoles). The labeling of the peptide conjugates with ^{68}Ga was carried out in a microwave monomodal oven. The UV-radio-HPLC analysis method developed for this study was accomplished within 10 min allowing fast quality control (QC) of the imaging agents prior to the application (**Figure 2**). The original DOTA-RGD and DOTA-DGF peptide conjugates were analyzed by UV-RP-HPLC with one and two UV-signals detected, respectively, for DOTA-RGD (t_R = 6.19 ± 0.03 min) and DOTA-DGF (t_{R1} = 6.12 ± 0.03 min and t_{R2} = 6.30 ± 0.04 min with ratio of 7.4 for the t_{R2}/t_{R1}).

Authentic reference comprising stable ^{69,71}Ga-(III) isotopes was synthesized under the same conditions as its radioactive counterpart. There were two UV signals with the first one corresponding to the authentic DOTA-RGD (t_R = 6.19 min) and the second one to ^{69,71}Ga-DOTA-RGD (t_R = 6.35 min). The radioactivity signal had t_R = 6.45 min. To confirm the HPLC UV-chromatogram signals another HPLC run of the sample spiked with DOTA-RGD was conducted. To confirm the HPLC UV-chromatogram signals ^{69,71}Ga-DOTA-RGD concentration dependent st-

20
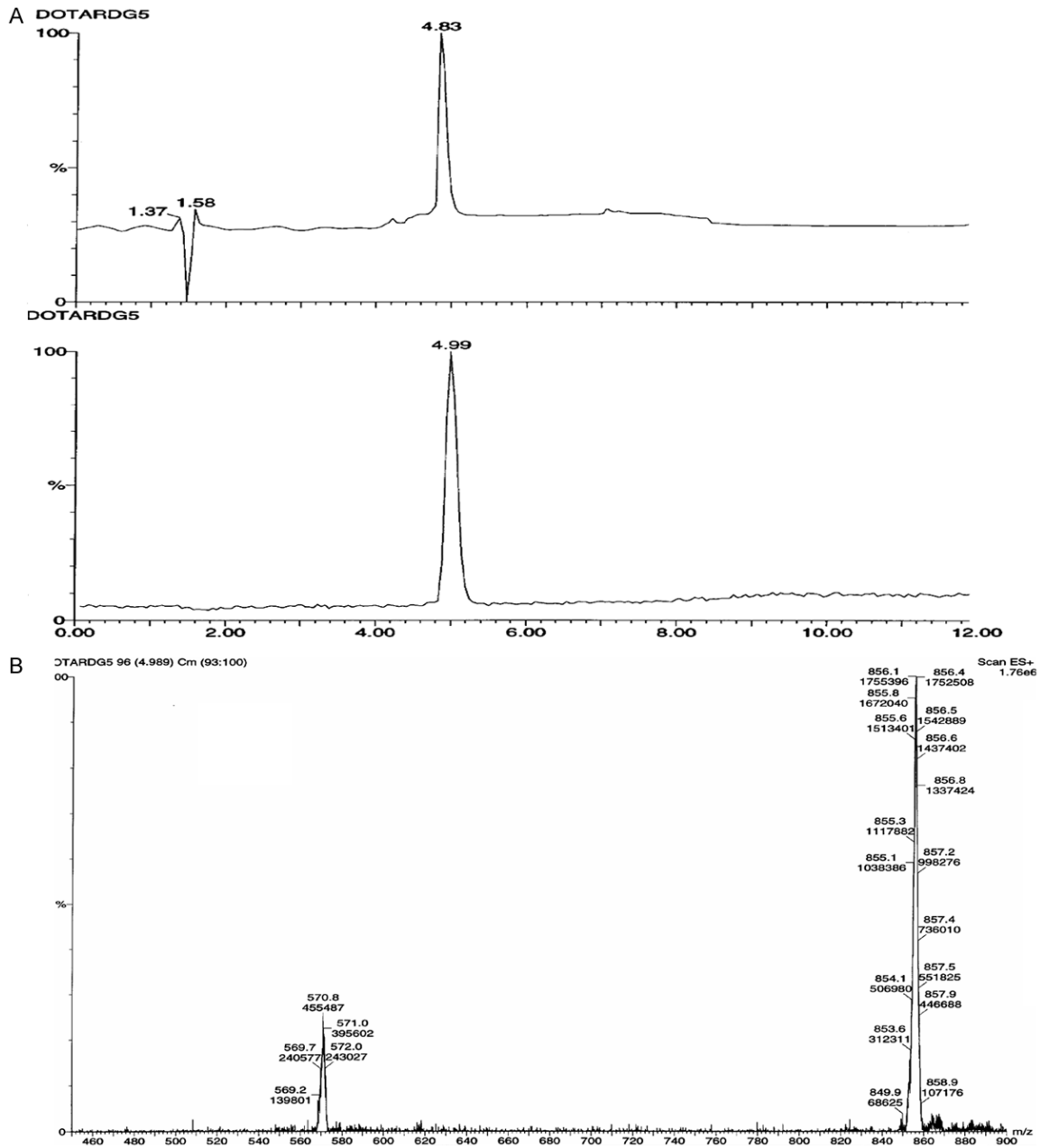
Figure 3. Electrospray ionization mass-spectrometry results of ^{69,71}Ga-DOTA-RGD analysis: A: The UV-chromatogram of a liquid chromatography separation (upper panel) and total ion chromatogram (lower panel); B: The corresponding mass spectrum.

udy was carried out. The area of the signal corresponding to ^{69,71}Ga-DOTA-RGD was increasing with the increasing concentration of the analyte. The identity of the compounds was confirmed by LC-ESI-MS. Double and triple charged ions at m/z: 857 [M+2H]$^{2+}$ and 571 [M+3H]$^{3+}$ were detected for ^{69,71}Ga-RGD (**Figure 3B**). In the case of the gallium stable isotope complexation, the product consisted of pure ^{69,71}Ga-

DOTA-RGD. In the case of ^{68}Ga complexation, the product consists of [^{68}Ga]Ga-DOTA-RGD and DOTA-RGD. The HPLC samples of the tracer preparations were spiked with DOTA-RGD to avoid t$_R$ discrepancies.

To check the stability of DOTA-RGD under microwave heating condition, blank experiments were performed and the stability of the peptide

[^{68}Ga]Ga-DOTA-RGD   **[^{68}Ga]Ga-DOTA-DGF**
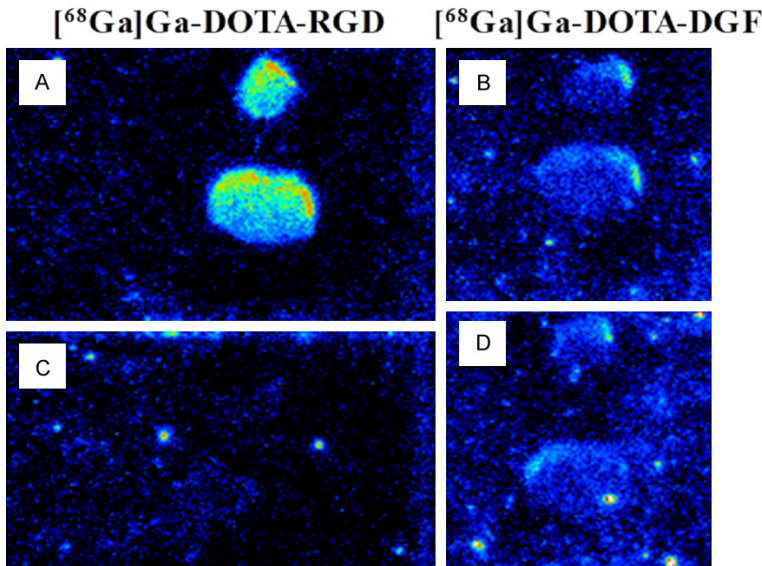
Figure 4. A representative autoradiogram of frozen section autoradiography of Lewis Lung carcinoma tumors incubated with 5-10 nM [^{68}Ga]Ga-DOTA-RGD (A, left panel) and [^{68}Ga]Ga-DOTA-DGF (B, right panel). The blocking with 5-15 µM NC-10071 resulted in the absence of [^{68}Ga]Ga-DOTA-RGD uptake (C, left panel). There was no difference in the uptake of [^{68}Ga]Ga-DOTA-DGF in the total binding (B) and blocking with NC-10071 experiments (D).
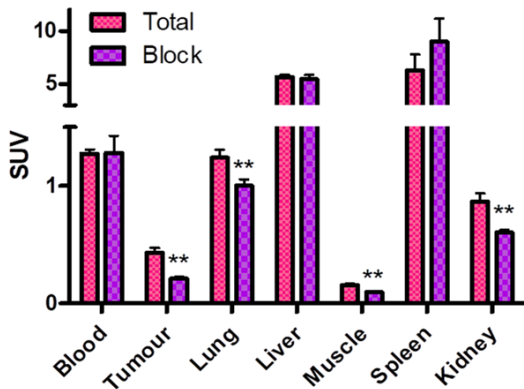
Figure 5. [^{68}Ga]Ga-DOTA-RGD uptake in C57Bl/6J mice with a subcutaneous LL2 tumor reported as SUVs with SEM for tumor and different organs (n = 3). **indicate P < 0.01.

conjugate was monitored by UV-HPLC and LC-ESI-MS. DOTA-RDG was stable both in water and in the reaction solution under microwave heating. No additional signals were detected in the stability study.

Lewis lung carcinoma model

Frozen section autoradiography: The incubation of frozen tumor sections with 10 nM [^{68}Ga]Ga-DOTA-RGD demonstrated specific binding in experiments wherein the binding was preclud-ed by excess of NC-100717 and only unspecific binding of [^{68}Ga]Ga-DOTA-DGF was observed wherein the blocking effect could not be achieved using excess of NC-100717 (**Figure 4**).

Organ distribution: The ex vivo organ distribution of [^{68}Ga]Ga-DOTA-RGD was investigated in LL2 tumor xenograft mice (**Figure 5**). The specificity of the tracer uptake was controlled in the presence of excess of NC-100717 (**Figure 5**). The biodistribution was characterized by fast renal clearance from blood. The accumulation in the spleen and liver was the highest followed by lung and kidney. The blocking of [^{68}Ga]Ga-DOTA-RGD with unlabeled NC-100717 showed that activity in blood and liver was not affected by the unlabeled peptide but lung and muscle uptake was reduced in similar manner.

Whole body autoradiography: Distribution of [^{18}F]FDG in tumor bearing mice shows a central defect in uptake indicating a central necrosis (**Figure 6B**). The accumulation of [^{68}Ga]Ga-DOTA-RGD is less pronounced than that of [^{18}F]FDG and can be observed to be higher at the rim of the tumor (**Figure 6A**). This uptake at the rim can be explained by neo-vascularization or representing activity in the blood vessels at the rim or a combination of the two tumors.

Animal PET imaging and kinetic data: The fast excretion of [^{68}Ga]Ga-DOTA-RGD resulted in high accumulation of the radioactivity in the urinary bladder and it was difficult to outline the tumor (**Figure 7A**). The radioactivity was accumulated in the bladder within 15 min while there was only minor retention of the radioactivity in the kidney (**Figure 7B**). Retention in the tumor was observed for at least 30 min. The two investigated animals demonstrated similar distribution pattern. The central uptake defect of [^{18}F]FDG observed in tape section autoradiograms is also observed in the animal PET image (**Figure 7C**). The time-activity-curves demonstrated also for [^{18}F]FDG fast excretion to the
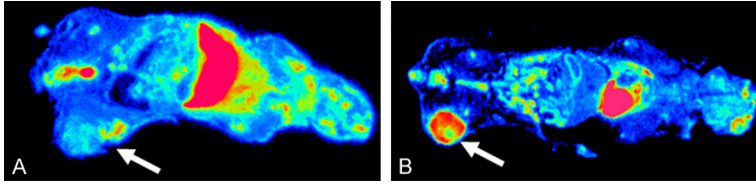
Figure 6. Ex vivo whole body autoradiography (30 μm sections) of C57Bl/6J mice with a subcutaneous LL2 tumor performed one hour post administration of 3 MBq of [^{68}Ga]Ga-DOTA-RGD (A) and [^{18}F]FDG (B). White arrows point at LL2 tumor uptake.
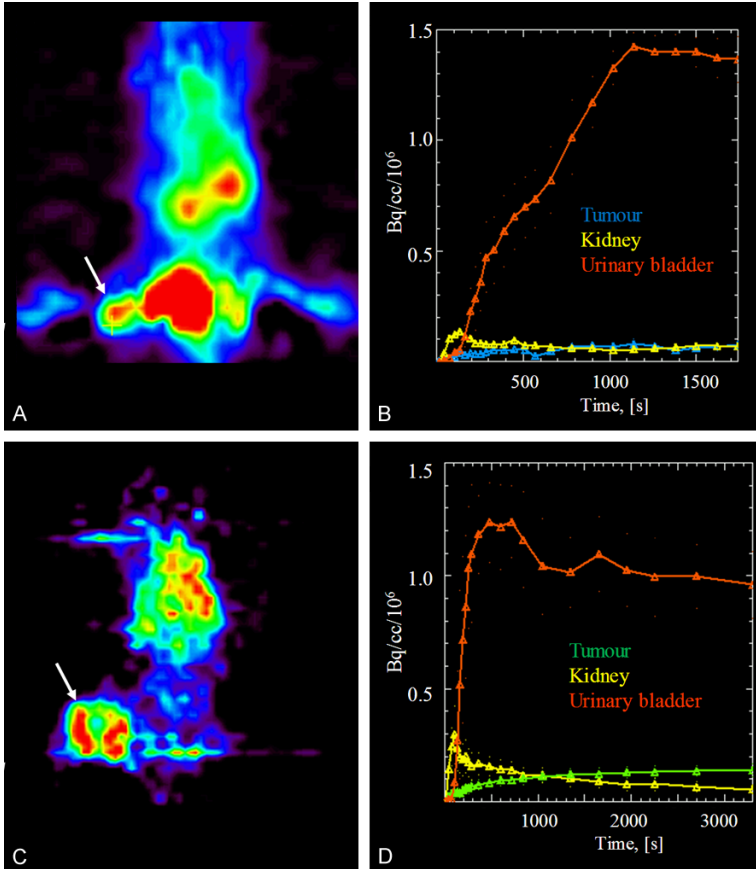
Figure 7. Animal summation PET images of dynamic scanning after administration of 3 MBq of [^{68}Ga]Ga-DOTA-RGD (A) and 2.5 MBq of [^{18}F]FDG (C) to C57Bl/6J mice wherein the white arrows point at the subcutaneous LL2 tumors. The respective time-activity curves demonstrate fast accumulation in urinary bladder and retention in the tumor for both [^{68}Ga]Ga-DOTA-RGD (B) and [^{18}F]FDG (D).

urinary bladder and retention of the radioactivity in the tumor.

Non-human primate

PET imaging and in vivo blocking of [68Ga]Ga-DOTA-RGD uptake with NC-100717: The whole body scans were performed after administration of [^{18}F]FDG (**Figure 8A**) and [^{68}Ga]Ga-DOTA-

RGD (**Figure 8B**). The former was accumulated mostly in the brain and urinary bladder. The uptake in the uterus was low and throughout the organ. The whole body organ distribution of [^{68}Ga]Ga-DOTA-RGD demonstrated accumulation in the wall of the uterus, probably indicating vascularization (**Figure 8B**). The highest uptake was observed at the upper pole of the uterus. Computed tomography imaging confirmed the formation of a neoplasm with increased uterus wall thickness from 5 mm to 7 mm within 3 months.

Upon the co-injection of NC-100717, the accumulation of [^{68}Ga]Ga-DOTA-RGD in uterus was markedly inhibited (**Figure 9A**), the excretion of [^{68}Ga]Ga-DOTA-RGD increased (**Figure 9B**), and the plasma half-life was prolonged (**Figure 9C**). The blood clearance kinetics was best described by a bi-exponential function with slow and fast phases of half-life values of 24.6/1.1 and 26.4/1.9 min (R^2 = 0.9999 and 0.9978), respectively for the animals scanned at the baseline without administration of the blocking NC-100-717, and the animals scanned after the administration of NC-100717 (1 mg/kg) (**Figure 9C**).

Discussion

One of the basic requirements of the personalized medicine is the quantification of the disease [56]. The molecular imaging and, in particular PET provides the possibility and tool for the selection of patients, dosimetry, treatment planning and monitoring of the response to the therapy. Such application of PET for the targeted imaging of e.g. receptors requires sufficiently high SRA of the imaging agent [57]. The requirement is dictated by biological factors such as limited number of targets, e.g. recep-
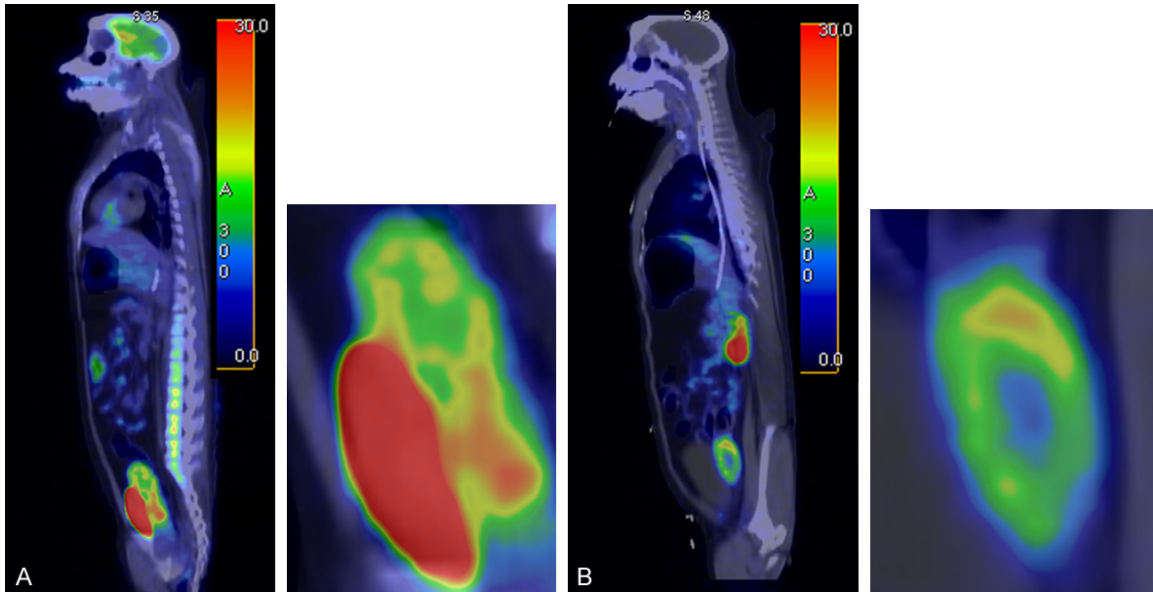
Figure 8. A: Sagittal PET/CT fusion image of [^{18}F]FDG distribution in a non-human primate showing high uptake in the uterus and bladder (240 s/bed scanning started 130 min post injection). B: Sagittal PET/CT fusion image of [^{68}Ga]Ga-DOTA-RGD distribution in a non-human primate showing distinct accumulation of the radioactivity in the wall of uretus (240 s/bed scanning started 20 min post injection).
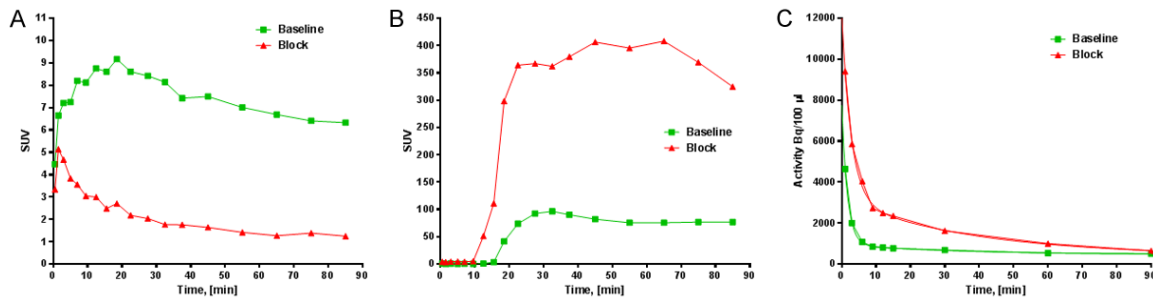
Figure 9. Time-activity-curves demonstrating: A: Accumulation of [^{68}Ga]Ga-DOTA-RGD in the upper pole of the uterus in a non-human primate before and after administration of NC-100717 (1 mg/kg); B: Excretion of [^{68}Ga]Ga-DOTA-RGD to urine in a non-human primate before and after administration of NC-100717 (1 mg/kg); C: [^{68}Ga]Ga-DOTA-RGD radioactivity in blood plasma in a non-human primate before and after administration of NC-100717 (1 mg/kg).

tors and pharmacological side effects. In particular, due to competition with the labeled peptide for the same receptor, the presence of unlabeled peptide may have a negative effect on the percent dose uptake of radioactivity.

Various agents for imaging and quantification of angiogenesis were developed and tested preclinically and clinically targeting integrin receptors, vascular endothelial growth factor (VEGF) receptors, MMP-9, and aminopeptidase N [58, 59]. A number of tracers based on VEGF analogues and labeled with [99m]Tc [60], [68]Ga [61], [64]Cu [62, 63] were assessed preclinically showing such shortcomings as relatively slow

blood and tissue clearance as well as high kidney uptake. Smaller peptides targeting integrin receptors demonstrated faster target localization and clearance from blood and healthy tissue and thus were found preferable as compared to VEGF based agents. Ligands comprising arginine-glycine-aspartic acid (RGD) sequence for binding to integrin receptors constitute the largest and most thoroughly investigated group of imaging agents for angiogenesis.

A versatile RGD peptide scaffold with nanomolar affinity (K_i and IC_{50}) for $\alpha_v\beta_3$ ranging between 0.75-8.2 nM for various analogues was developed [49, 54]. Three analogues with basic

cyclic structure containing eight amino acid residues, ethylene glycol linker, and DOTA chelator moiety were used in this study. DOTA-RGD had RGD motif for the specific binding to $\alpha_v\beta_3$ receptors while DOTA-DGF had the same amino acid residues however with altered sequence exchanging RGD motif to DGF one in order to assess the necessity of RGD motif for receptor binding (**Figure 1B**, **1C**). NC-100717 analogue used in blocking and competition assays had the same constitution as DOTA-RGD except for the absence of the chelator moiety (**Figure 1A**).

Radiochemistry

The positron-emitting ^{68}Ga radionuclide is of great practical interest for clinical PET. The ^{68}Ga is a generator produced nuclide and does not require cyclotron on site. The short half-life of [68]Ga ($t_{1/2}$ = 68 min) permits application of ^{68}Ga radioactivity amount sufficient for high quality images while maintaining relatively low radiation dose to the patient. The requirement of high SRA can be fulfilled if the incorporation of ^{68}Ga is nearly quantitative, the amount of the peptide conjugate is low, and the tracer does not necessitate purification. All requirements were met in this study wherein DOTA-RGD and DOTA-DGF were labeled with ^{68}Ga radioactivity incorporation of over 95% (97 ± 2%, n = 11) and high reproducibility of 100% success rate. The amount of the precursor was less than 5 nanomoles. The high radioactivity incorporation resulting in sufficiently pure product and the use of biologically compatible HEPES buffer allowed omission of the purification step. The proposed labeling technique was time efficient due to the elimination of the product purification step and fast microwave heating (1 min). No degradation of the peptides was observed in concordance with previously published reports on the applicability of microwave heating for labeling synthesis of various peptides and oligonucleotides [55, 57]. Another factor that contributed to the improved SRA was the introduction of preconcentration/purification of the generator eluate [13]. The procedure was based on anion exchange chromatography allowing preconcentration and purification of ^{68}Ga obtained from one or several generators, and resulting in considerable reduction of the generator eluate volume and enhancement of ^{68}Ga concentration. This labeling method combining microwave heating and preconcentration of the generator eluate demonstrated

promising results earlier [13, 24, 55, 57, 64-74], and was proved to be useful in the present study providing sufficiently high SRA (152 ± 32 MBq/nmol) relevant to the respective affinity values of the peptides. One more factor that contributed to the improvement of SRA was the short time of fast quality control method (10 min) allowing the overall tracer preparation time reduction to 20 min.

The introduction of the purification and concentration step combined with microwave heating may have very positive impact on the further utilization of ^{68}Ga in nuclear medicine in general. The generator eluate preconcentration allowed excellent ^{68}Ga radioactivity economy that potentially could prolong the shelf-life of a 50 mCi generator for up to 2 years for clinical use, especially considering harvest of the eluates from several generators wherein the preconcentration would provide the same small final volume (200-300 µL) and increased radioactivity amount. Moreover, the proposed generator eluate preconcentration technique was suited for automation [75, 76].

Biological assay

Analogues based on the RGD peptide scaffold were previously labeled with ^{18}F and ^{99m}Tc and demonstrated promising results clinically. [^{18}F] AH111585 selectively targeting $\alpha_v\beta_5$ and $\alpha_v\beta_3$ was investigated in breast cancer patients [49, 77], in melanoma and renal tumors [78], and antiangiogenic therapy monitoring [33, 79-81]. The agent was safe, metabolically stable, and able to detect lesions, however high background uptake in normal liver masked the liver metastases. Another analogue of this scaffold, [^{99m}Tc]NC100692, demonstrated detection rate of 86% in 20 patients with breast cancer [51]. No adverse effects were observed however clearance from the blood and healthy tissue was slow deteriorating the contrast of the images.

The results were promising, however the necessity of cyclotron for ^{18}F production and rather complex chemistry results in poor clinical availability and higher costs. It is worth mentioning that from the point of view of radiation dose [18]F- and ^{68}Ga-based tracers demonstrate comparable results despite the higher positron energy of [68]Ga [43, 53]. The relatively cheap and readily available from a simple generator system

[68]Ga as well as possibility of production automation and kit type tracer production make ^{68}Ga-based analogues more attractive. Similar production mode is provided by [99m]Tc [82, 83], however ^{68}Ga/PET offers advantage of higher sensitivity, resolution as well as accurate quantitation, and thus personalized medicine potential. The escalating appreciation of ^{68}Ga advantages is reflected in the increasing number of clinical studies using various RGD analogues [53, 84-88].

The potential shortcomings with radiolabeled RGD analogues were associated with slow blood and tissue clearance and accumulation in liver, intestine, bladder, and kidney. This study was designed to investigate the imaging potential of [^{68}Ga]Ga-DOTA-RGD in NHP taking advantage of physiological similarity between humans and NHPs providing superior validity of the experimental results as compared to those obtained in rodents. Nevertheless, the preliminary biological assessment was conducted in vitro and in vivo in rodents, prior to NHPs.

Organ distribution in rodents: The organ distribution of [^{68}Ga]Ga-DOTA-RGD and [^{68}Ga]Ga-DOTA-DGF was previously studied in healthy rats showing fast blood and tissue clearance, fast excretion and relatively low kidney uptake (SUVs) [21]. The ex vivo organ distribution of [^{68}Ga]Ga-DOTA-RGD in mice bearing LL2 xenografts in this study demonstrated somewhat higher uptake (SUVs) in blood, liver and spleen that can be attributed to the difference in species. In contrast to these studies, the kidney uptake prevailed in the study of atherosclerotic plaques in LDLR/ApoB48 mice [16]. The uptake in the LL2 tumor was precluded by 50% using excess of pre-administered NC-100717, while it was not affected in liver, spleen, and blood (**Figure 5**). Another analogue labeled with [99m]Tc (^{99m}Tc-NC100692) demonstrated similar results in murine model of angiogenesis induced by hindlimb ischemia and healthy rats [89, 90].

In vivo organ distribution kinetics of [^{68}Ga]Ga-DOTA-RGD in LL2 tumor bearing mice (**Figure 7A, 7B**) was studied and compared to that of [^{18}F]FDG (**Figure 7C, 7D**). The excretion to urine of [^{68}Ga]Ga-DOTA-RGD was fast and extensive, and it was difficult to outline the tumor due to the proximity to the urinary bladder. The radioactivity was accumulated in the bladder within 15 min while there was only minor retention of the radioactivity in the kidney (**Figure 7B**). The tumor accumulation was somewhat slower and lower for [^{68}Ga]Ga-DOTA-RGD. The central uptake defect of [^{18}F]FDG observed in tape section autoradiograms was also possible to delineate in the animal PET image (**Figure 7C**). The animals were sacrificed and whole body section autoradiography was performed for more detailed investigation of the radioactivity distribution throughout the tissue (**Figure 6**). Both [^{18}F]FDG and [^{68}Ga]Ga-DOTA-RGD images showed absence of the radioactivity in the central part of the tumor most probably due to necrosis (**Figure 6**).

The binding specificity of [^{68}Ga]Ga-DOTA-RGD was additionally confirmed in vitro in frozen sections of LL2 tumors wherein the tracer uptake was precluded by pre-incubation with excess of NC-100717 (**Figure 4A**, **4C**) while there was no difference in the uptake pattern of [^{68}Ga]Ga-DOTA-DGF with and without NC-100717 (**Figure 4B**, **4D**). The results imply that the specificity of the uptake was defined by the presence of RGD sequence in the peptide construct.

Organ distribution in non-human primate: The PET/CT examinations of a NHP showed accumulation in the uterus for both [^{68}Ga]Ga-DOTA-RGD and [^{18}F]FDG, the latter had however a much diffuser appearance (**Figure 8A**) while the former demonstrated very distinct uptake in the wall of the uterus with highest density in the upper pole (**Figure 8B**). The localization of [^{68}Ga]Ga-DOTA-RGD in the wall correlated with the findings of computed tomography imaging that showed formation of a neoplasm with increased uterus wall thickness from 5 mm to 7 mm within 3 months. The use of [^{68}Ga]Ga-DOTA-RGD may present some advantages over [^{18}F]FDG in specificity similarly to the observations in lung cancer diagnosis wherein the specificity of [^{68}Ga]Ga-NOTA-RGD$_2$ was found considerably higher than that of [^{18}F]FDG [86].

Apart from the excretion to urine, [^{68}Ga]Ga-DOTA-RGD uptake in the other tissues was negligible providing very low background (**Figure 8B**) and potentially high contrast images of lesion localization in organs. The in vivo blocking study with NC100717 demonstrated reduction of the uptake, especially in the upper pole of the uterus by approximately 70% confirming the specificity of the binding (**Figure 9A**). The

drastic increase of the radioactivity excretion to urine upon the blocking with NC100717 (**Figure 9B**) also indirectly indicates the binding specificity. The blockage of the binding target was reflected in the enhanced blood plasma levels and longer plasma half-life of [^{68}Ga] Ga-DOTA-RGD (**Figure 9C**). The difference in the background uptake between rodents (**Figure 7**) and NHP (**Figure 8**) was attributed to the difference between the species, and it stresses the importance of the validation of a tracer candidate in larger animals with physiology as similar to human one as possible very early in the tracer development process.

In summary, the binding specificity was confirmed in vitro in frozen sections of LL2 tumors, ex vivo and in vivo in C57B1/6J mice with LL2 xenografts, and in vivo in NHP. The comparison with [^{18}F]FDG organ distribution indirectly indicated the specificity of [^{68}Ga]Ga-DOTA-RGD action. Receptor mediated specific binding in combination with low background uptake in healthy organs observed in the NHP indicated strong potential of the agent for non-invasive in vivo localization and quantification of integrin receptor rich lesions.

Conclusion

The bicyclic octapeptide conjugates, DOTA-RGD and DOTA-DGF, were nearly quantitatively labeled with positron emitting radionuclide ^{68}Ga eluted from two generators. [^{68}Ga]Ga-DOTA-RGD demonstrated specific binding in the LL2 tumor model that could be precluded by excess of the blocking agent. The amino acid sequence related uptake mechanism could be shown by the absence of the blocking effect when using scrambled peptide conjugate, DOTA-DGF. The uptake in the wall of uterus in non-human primate most likely indicated neovascularisation and could partly be blocked. [^{68}Ga]Ga-DOTA-RGD has a potential to be a valuable tool in examining and quantifying various processes with a high degree of angiogenesis.

Acknowledgements

Disclosure of conflict of interest

None.

Address correspondence to: Dr. Irina Velikyan, PET-Center, Center for Medical Imaging, Uppsala University Hospital, SE-751 85 Uppsala, Sweden. Tel: +46 (0)70 4834137; Fax: +46 (0)18 6110619; E-mail: irina.velikyan@akademiska.se

References

[1] Folkman J. Tumor angiogenesis: therapeutic implications. N Engl J Med 1971; 285: 1182-1186.

[2] Bergstrom M, Grahnen A and Langstrom B. Positron emission tomography microdosing: a new concept with application in tracer and early clinical drug development. Eur J Clin Pharmacol 2003; 59: 357-366.

[3] Garner RC and Lappin G. The phase 0 microdosing concept. Br J Clin Pharmacol 2006; 61: 367-370.

[4] Velikyan I. Positron emitting [^{68}Ga]Ga-based imaging agents: chemistry and diversity. Med Chem 2011; 7: 338-372.

[5] Dijkgraaf I and Boerman OC. Radionuclide imaging of tumor angiogenesis. Cancer Biother Radiopharm 2009; 24: 637-647.

[6] Zhang Y, Yang Y and Cai W. Multimodality imaging of integrin alpha(v)beta(3) expression. Theranostics 2011; 1: 135-148.

[7] Janssen M, Oyen WJ, Massuger LF, Frielink C, Dijkgraaf I, Edwards DS, Radjopadhye M, Corstens FH and Boerman OC. Comparison of a monomeric and dimeric radiolabeled RGD-peptide for tumor targeting. Cancer Biother Radiopharm 2002; 17: 641-646.

[8] Liu S. Radiolabeled multimeric cyclic RGD peptides as integrin alphavbeta3 targeted radiotracers for tumor imaging. Mol Pharm 2006; 3: 472-487.

[9] Haubner R, Kuhnast B, Mang C, Weber WA, Kessler H, Wester HJ and Schwaiger M. [^{18}F] Galacto-RGD: synthesis, radiolabeling, metabolic stability, and radiation dose estimates. Bioconjug Chem 2004; 15: 61-69.

[10] Chen X, Park R, Shahinian AH, Bading JR and Conti PS. Pharmacokinetics and tumor retention of ^{125}I-labeled RGD peptide are improved by PEGylation. Nucl Med Biol 2004; 31: 11-19.

[11] Azad BB, Cho CF, Lewis JD and Luyt LG. Synthesis, radiometal labeling and in vitro evaluation of a targeted PPIX derivative. Appl Radiat Isot 2012; 70: 505-511.

[12] Simecek J, Zemek O, Hermann P, Wester HJ and Notni J. A monoreactive bifunctional triazacyclononane phosphinate chelator with high selectivity for gallium-68. ChemMedChem 2012; 7: 1375-1378.

[13] Velikyan I, Beyer GJ and Langstrom B. Micro-wave-supported preparation of ^{68}Ga-bioconjugates with high specific radioactivity. Bioconjug Chem 2004; 15: 554-560.

[14] Decristoforo C, Hernandez Gonzalez I, Carlsen J, Rupprich M, Huisman M, Virgolini I, Wester HJ and Haubner R. ^{68}Ga- and ^{111}In-labelled DOTA-RGD peptides for imaging of alphavbeta3 integrin expression. Eur J Nucl Med Mol Imaging 2008; 35: 1507-1515.

[15] Jeong JM, Hong MK, Chang YS, Lee YS, Kim YJ, Cheon GJ, Lee DS, Chung JK and Lee MC. Preparation of a promising angiogenesis PET imaging agent: Ga-68-labeled c(RGDyK)-iso-thiocyanatobenzyl-1,4,7-triazacyclononane-1,4,7-triacetic acid and feasibility studies in mice. J Nucl Med 2008; 49: 830-836.

[16] Haukkala J, Laitinen I, Luoto P, Iveson P, Wilson I, Karlsen H, Cuthbertson A, Laine J, Leppanen P, Yla-Herttula S, Knuuti J and Roivainen A. ^{68}Ga-DOTA-RGD peptide: biodistribution and binding into atherosclerotic plaques in mice. Eur J Nucl Med Mol Imaging 2009; 36: 2058-2067.

[17] Dumont RA, Deininger F, Haubner R, Maecke HR, Weber WA and Fani M. Novel ^{64}Cu- and ^{68}Ga-labeled RGD conjugates show improved PET imaging of alpha(nu)beta(3) integrin expression and facile radiosynthesis. J Nucl Med 2011; 52: 1276-1284.

[18] Knetsch PA, Petrik M, Griessinger CM, Rangger C, Fani M, Kesenheimer C, von Guggenberg E, Pichler BJ, Virgolini I, Decristoforo C and Haubner R. [^{68}Ga]NODAGA-RGD for imaging alphavbeta3 integrin expression. Eur J Nucl Med Mol Imaging 2011; 38: 1303-1312.

[19] Pohle K, Notni J, Bussemer J, Kessler H, Schwaiger M and Beer AJ. 68Ga-NODAGA-RGD is a suitable substitute for ^{18}F-Galacto-RGD and can be produced with high specific activity in a cGMP/GRP compliant automated process. Nucl Med Biol 2012; 39: 777-784.

[20] Ferreira CL, Yapp DT, Mandel D, Gill RK, Boros E, Wong MQ, Jurek P and Kiefer GE. ^{68}Ga small peptide imaging: comparison of NOTA and PCTA. Bioconjug Chem 2012; 23: 2239-2246.

[21] Blom E, Velikyan I, Estrada S, Hall H, Muhammad T, Ding C, Nair M and Langstrom B. ^{68}Ga-labeling of RGD peptides and biodistribution. Int J Clin Exp Med 2012; 5: 165-172.

[22] Notni J, Simecek J, Hermann P and Wester HJ. TRAP, a powerful and versatile framework for Gallium-68 Radiopharmaceuticals. Chem Eur J 2011; 17: 14718-14722.

[23] Laitinen I, Notni J, Pohle K, Rudelius M, Farrell E, Nekolla SG, Henriksen G, Neubauer S, Kessler H, Wester HJ and Schwaiger M. Comparison of cyclic RGD peptides for αvβ3 integrin detection in a rat model of myocardial infarction. EJNMMI Res 2013; 3: 38.

[24] Velikyan I, Långström B, Bergström M and Lindhe Ö. ^{68}Ga-labeled peptide-based radiopharmaceuticals. WO/2008/026040, 2008; USA.

[25] Liu ZF, Yan YJ, Liu SL, Wang F and Chen XY. F-18, Cu-64, and Ga-68 labeled RGD-bombesin heterodimeric peptides for PET imaging of breast cancer. Bioconjugate Chem 2009; 20: 1016-1025.

[26] Liu Z, Niu G, Wang F and Chen X. ^{68}Ga-labeled NOTA-RGD-BBN peptide for dual integrin and GRPR-targeted tumor imaging. Eur J Nucl Med Mol Imaging 2009; 36: 1483-1494.

[27] Ma MT, Neels OC, Denoyer D, Roselt P, Karas JA, Scanlon DB, White JM, Hicks RJ and Donnelly PS. Gallium-68 complex of a macrobicyclic cage amine chelator tethered to two integrin-targeting peptides for diagnostic tumor imaging. Bioconjug Chem 2011; 22: 2093-2103.

[28] Eo JS, Paeng JC, Lee S, Lee YS, Jeong JM, Kang KW, Chung JK and Lee DS. Angiogenesis imaging in myocardial infarction using ^{68}Ga-NOTA-RGD PET: characterization and application to therapeutic efficacy monitoring in rats. Coron Artery Dis 2013; 24: 303-311.

[29] Li ZB, Chen K and Chen X. ^{68}Ga-labeled multimeric RGD peptides for microPET imaging of integrin alpha(v)beta (3) expression. Eur J Nucl Med Mol Imaging 2008; 35: 1100-1108.

[30] Dijkgraaf I, Yim CB, Franssen GM, Schuit RC, Luurtsema G, Liu S, Oyen WJ and Boerman OC. PET imaging of alphavbeta integrin expression in tumours with Ga-labelled mono-, di- and tetrameric RGD peptides. Eur J Nucl Med Mol Imaging 2011; 38: 128-137.

[31] Singh AN, Liu W, Hao GY, Kumar A, Gupta A, Oz OK, Hsieh JT and Sun XK. Multivalent bifunctional chelator scaffolds for gallium-68 based positron emission tomography imaging probe design: signal amplification via multivalency. Bioconjug Chem 2011; 22: 1650-1662.

[32] Liu Z, Niu G, Shi J, Liu S, Wang F and Chen X. ^{68}Ga-labeled cyclic RGD dimers with Gly3 and PEG4 linkers: promising agents for tumor integrin alphavbeta3 PET imaging. Eur J Nucl Med Mol Imaging 2009; 36: 947-957.

[33] Morrison MS, Ricketts SA, Barnett J, Cuthbertson A, Tessier J and Wedge SR. Use of a novel Arg-Gly-Asp radioligand, F-18-AH111585, to determine changes in tumor vascularity after antitumor therapy. J Nucl Med 2009; 50: 116-122.

[34] Guo J, Lang L, Hu S, Guo N, Zhu L, Sun Z, Ma Y, Kiesewetter DO, Niu G, Xie Q and Chen X. Comparison of three dimeric ^{18}F-AlF-NOTA-RGD tracers. Mol Imaging Biol 2013; 1-10.

[35] Lang L, Li W, Guo N, Ma Y, Zhu L, Kiesewetter DO, Shen B, Niu G and Chen X. Comparison study of [^{18}F]FAl-NOTA-PRGD2, [^{18}F] FPPRGD2,

and [^{68}Ga]Ga-NOTA-PRGD2 for PET imaging of u87mg tumors in mice. Bioconjug Chem 2011; 22: 2415-2422.

[36] Gao H, Lang L, Guo N, Cao F, Quan Q, Hu S, Kiesewetter DO, Niu G and Chen X. PET imaging of angiogenesis after myocardial infarction/reperfusion using a one-step labeled integrin-targeted tracer ^{18}F-AlF-NOTA-PRGD2. Eur J Nucl Med Mol Imaging 2012; 39: 683-692.

[37] Bach-Gansmo T, Bogsrud TV and Skretting A. Integrin scintimammography using a dedicated breast imaging, solid-state gamma-camera and ^{99m}Tc-labelled NC100692. Clin Physiol Funct Imaging 2008; 28: 235-239.

[38] Decristoforo C, Faintuch-Linkowski B, Rey A, von Guggenberg E, Rupprich M, Hernandez-Gonzales I, Rodrigo T and Haubner R. [^{99m}Tc]HYNIC-RGD for imaging integrin alphavbeta3 expression. Nucl Med Biol 2006; 33: 945-952.

[39] Chen X, Liu S, Hou Y, Tohme M, Park R, Bading JR and Conti PS. MicroPET imaging of breast cancer alphav-integrin expression with ^{64}Cu-labeled dimeric RGD peptides. Mol Imaging Biol 2004; 6: 350-359.

[40] Jacobson O, Zhu L, Niu G, Weiss ID, Szajek LP, Ma Y, Sun X, Yan Y, Kiesewetter DO, Liu S and Chen X. MicroPET imaging of integrin alphavbeta3 expressing tumors using [89]Zr-RGD peptides. Mol Imaging Biol 2011; 13: 1224-1233.

[41] Knetsch PA, Petrik M, Rangger C, Seidel G, Pietzsch HJ, Virgolini I, Decristoforo C and Haubner R. [^{68}Ga]NS3-RGD and [^{68}Ga] Oxo-DO3A-RGD for imaging αvβ3 integrin expression: synthesis, evaluation, and comparison. Nucl Med Biol 2013; 40: 65-72.

[42] Cai H and Conti PS. RGD-based PET tracers for imaging receptor integrin $\alpha_v\beta_3$ expression. J Labelled Compd Radiopharm 2013; 56: 264-279.

[43] Beer AJ, Haubner R, Wolf I, Goebel M, Luderschmidt S, Niemeyer M, Grosu AL, Martinez MJ, Wester HJ, Weber WA and Schwaiger M. PET-based human dosimetry of ^{18}F-galacto-RGD, a new radiotracer for imaging alpha v beta3 expression. J Nucl Med 2006; 47: 763-769.

[44] Beer AJ, Grosu AL, Carlsen J, Kolk A, Sarbia M, Stangier I, Watzlowik P, Wester HJ, Haubner R and Schwaiger M. [^{18}F]Galacto-RGD positron emission tomography for imaging of $\alpha_v\beta_3$ expression on the neovasculature in patients with squamous cell carcinoma of the head and neck. Clin Cancer Res 2007; 13: 6610-6616.

[45] Schnell O, Krebs B, Carlsen J, Miederer I, Goetz C, Goldbrunner RH, Wester HJ, Haubner R, Popperl G, Holtmannspotter M, Kretzschmar HA, Kessler H, Tonn JC, Schwaiger M and Beer AJ. Imaging of integrin alpha(v)beta(3) expression in patients with malignant glioma by [^{18}F]

Galacto-RGD positron emission tomography. Neuro Oncol 2009; 11: 861-870.

[46] Beer AJ, Lorenzen S, Metz S, Herrmann K, Watzlowik P, Wester HJ, Peschel C, Lordick F and Schwaiger M. Comparison of integrin alphaVbeta3 expression and glucose metabolism in primary and metastatic lesions in cancer patients: a PET study using ^{18}F-galacto-RGD and ^{18}F-FDG. J Nucl Med 2008; 49: 22-29.

[47] Haubner R, Weber WA, Beer AJ, Vabuliene E, Reim D, Sarbia M, Becker KF, Goebel M, Hein R, Wester HJ, Kessler H and Schwaiger M. Noninvasive visualization of the activated alphavbeta3 integrin in cancer patients by positron emission tomography and [^{18}F]Galacto-RGD. PLoS Med 2005; 2: e70.

[48] McParland BJ, Miller MP, Spinks TJ, Kenny LM, Osman S, Khela MK, Aboagye E, Coombes RC, Hui AM and Cohen PS. The biodistribution and radiation dosimetry of the Arg-Gly-Asp peptide ^{18}F-AH111585 in healthy volunteers. J Nucl Med 2008; 49: 1664-1667.

[49] Kenny LM, Coombes RC, Oulie I, Contractor KB, Miller M, Spinks TJ, McParland B, Cohen PS, Hui AM, Palmieri C, Osman S, Glaser M, Turton D, Al-Nahhas A and Aboagye EO. Phase I trial of the positron-emitting Arg-Gly-Asp (RGD) peptide radioligand ^{18}F-AH111585 in breast cancer patients. J Nucl Med 2008; 49: 879-886.

[50] Sivolapenko GB, Skarlos D, Pectasides D, Stathopoulou E, Milonakis A, Sirmalis G, Stuttle A, Courtenay-Luck NS, Konstantinides K and Epenetos AA. Imaging of metastatic melanoma utilising a technetium-99m labelled RGD-containing synthetic peptide. Eur J Nucl Med 1998; 25: 1383-1389.

[51] Bach-Gansmo T, Danielsson R, Saracco A, Wilczek B, Bogsrud TV, Fangberget A, Tangerud A and Tobin D. Integrin receptor imaging of breast cancer: a proof-of-concept study to evaluate ^{99m}Tc-NC100692. J Nucl Med 2006; 47: 1434-1439.

[52] Beer AJ, Haubner R, Goebel M, Luderschmidt S, Spilker ME, Wester HJ, Weber WA and Schwaiger M. Biodistribution and pharmacokinetics of the alphavbeta3-selective tracer ^{18}F-galacto-RGD in cancer patients. J Nucl Med 2005; 46: 1333-1341.

[53] Kim JH, Lee JS, Kang KW, Lee HY, Han SW, Kim TY, Lee YS, Jeong JM and Lee DS. Whole-body distribution and radiation dosimetry of ^{68}Ga-NOTA-RGD, a positron emission tomography agent for angiogenesis imaging. Cancer Biother Radiopharm 2012; 27: 65-71.

[54] Indrevoll B, Kindberg GM, Solbakken M, Bjurgert E, Johansen JH, Karlsen H, Mendizabal M and Cuthbertson A. NC-100717: a versatile

RGD peptide scaffold for angiogenesis imaging. Bioorg Med Chem Lett 2006; 16: 6190-6193.

[55] Velikyan I. Synthesis, characterization and application of ^{68}Ga-labelled macromolecules Doctorate thesis 2005; http://urn.kb.se/resolve?urn=urn:nbn:se:uu:diva-5876.

[56] Eckelman WC, Reba RC and Kelloff GJ. Targeted imaging: an important biomarker for understanding disease progression in the era of personalized medicine. Drug Discov Today 2008; 13: 748-759.

[57] Velikyan I, Beyer GJ, Bergstrom-Pettermann E, Johansen P, Bergstrom M and Langstrom B. The importance of high specific radioactivity in the performance of ^{68}Ga-labeled peptide. Nucl Med Biol 2008; 35: 529-536.

[58] Velikyan I. Continued rapid growth in Ga applications: update 2013 to June 2014. J Labelled Comp Radiopharm 2015; 99-121.

[59] Haubner R, Beer AJ, Wang H and Chen X. Positron emission tomography tracers for imaging angiogenesis. Eur J Nucl Med Mol Imaging 2010; 37 Suppl 1: S86-103.

[60] Blankenberg FG, Levashova Z, Sarkar SK, Pizzonia J, Backer MV and Backer JM. Noninvasive assessment of tumor VEGF receptors in response to treatment with pazopanib: a molecular imaging study. Transl Oncol 2010; 3: 56-64.

[61] Blom E, Velikyan I, Monazzam A, Razifar P, Nair M, Razifar P, Vanderheyden JL, Krivoshein AV, Backer M, Backer J and Långström B. Synthesis and characterization of scVEGF-PEG-[^{68}Ga]NOTA and scVEGF-PEG-[^{68}Ga]DOTA PET tracers. J Labelled Comp Radiopharm 2011; 54: 685-692.

[62] Cai W, Chen K, Mohamedali KA, Cao Q, Gambhir SS, Rosenblum MG and Chen X. PET of vascular endothelial growth factor receptor expression. J Nucl Med 2006; 47: 2048-2056.

[63] Chen K, Cai W, Li ZB, Wang H and Chen X. Quantitative PET imaging of VEGF receptor expression. Mol Imaging Biol 2009; 11: 15-22.

[64] Bergstrom SK, Edenwall N, Laven M, Velikyan I, Langstrom B and Markides KE. Polyamine deactivation of integrated poly(dimethylsiloxane) structures investigated by radionuclide imaging and capillary electrophoresis experiments. Anal Chem 2005; 77: 938-942.

[65] Blom E, Langstrom B and Velikyan I. ^{68}Ga-Labeling of biotin analogues and their characterization. Bioconjug Chem 2009; 20: 1146-1151.

[66] Lavén M, Wallenborg S, Velikyan I, Bergstrom S, Djodjic M, Ljung J, Berglund O, Edenwall N, Markides KE and Langstrom B. Radionuclide imaging of miniaturized chemical analysis systems. Anal Chem 2004; 76: 7102-7108.

[67] Laven M, Velikyan I, Djodjic M, Ljung J, Berglund O, Markides K, Langstrom B and Wallenborg S. Imaging of peptide adsorption to microfluidic channels in a plastic compact disc using a positron emitting radionuclide. Lab on a Chip 2005; 5: 756-763.

[68] Lendvai G, Monazzam A, Velikyan I, Eriksson B, Josephsson R, Langstrom B, Bergstrom M and Estrada S. Non-hybridization saturable mechanisms play a role in the uptake of ^{68}Ga-labeled LNA-DNA mixmer antisense oligonucleotides in rats. Oligonucleotides 2009; 19: 223-232.

[69] Lendvai G, Velikyan I, Bergstrom M, Estrada S, Laryea D, Valila M, Salomaki S, Langstrom B and Roivainen A. Biodistribution of ^{68}Ga-labelled phosphodiester, phosphorothioate, and 2'-O-methyl phosphodiester oligonucleotides in normal rats. Eur J Pharm Sci 2005; 26: 26-38.

[70] Lendvai G, Velikyan I, Estrada S, Eriksson B, Langstrom B and Bergstrom M. Biodistribution of ^{68}Ga-labeled LNA-DNA mixmer antisense oligonucleotides for rat chromogranin-A. Oligonucleotides 2008; 18: 33-49.

[71] Roivainen A, Tolvanen T, Salomaki S, Lendvai G, Velikyan I, Numminen P, Valila M, Sipila H, Bergstrom M, Harkonen P, Lonnberg H and Langstrom B. ^{68}Ga-labeled oligonucleotides for in vivo imaging with PET. J Nucl Med 2004; 45: 347-355.

[72] Velikyan I, Lendvai G, Valila M, Roivainen A, Yngve U, Bergstrom M and Langstrom B. Microwave accelerated ^{68}Ga-labelling of oligonucleotides. Journal of Labelled Compounds and Radiopharmaceuticals 2004; 47: 79-89.

[73] Velikyan I and Långström B. Microwave method for preparing radiolabelled gallium complexes. WO/2004/089425, 2004; USA.

[74] Velikyan I, Sundberg AL, Lindhe O, Hoglund AU, Eriksson O, Werner E, Carlsson J, Bergstrom M, Langstrom B and Tolmachev V. Preparation and evaluation of ^{68}Ga-DOTA-hEGF for visualization of EGFR expression in malignant tumors. J Nucl Med 2005; 46: 1881-1888.

[75] Gebhardt P, Opfermann T and Saluz HP. Computer controlled Ga-68 milking and concentration system. Appl Radiat Isot 2010; 68: 1057-1059.

[76] Velikyan I, Sundin A, Eriksson B, Lundqvist H, Sorensen J, Bergstrom M and Langstrom B. In vivo binding of [^{68}Ga]-DOTATOC to somatostatin receptors in neuroendocrine tumours-impact of peptide mass. Nucl Med Biol 2010; 37: 265-275.

[77] Tomasi G, Kenny L, Mauri F, Turkheimer F and Aboagye EO. Quantification of receptor-ligand binding with [^{18}F]fluciclatide in metastatic breast cancer patients. Eur J Nucl Med Mol Imaging 2011; 38: 2186-2197.

[78] Mena E, Owenius R, Turkbey B, Sherry R, Bratslavsky G, Macholl S, Miller MP, Somer EJ, Lindenberg L, Adler S, Shih J, Choyke P and Kurdziel K. [18F]fluciclatide in the in vivo evaluation of human melanoma and renal tumors expressing alphavbeta 3 and alpha vbeta 5 integrins. Eur J Nucl Med Mol Imaging 2014; 41: 1879-1888.

[79] Beer AJ and Schwaiger M. PET of alphavbeta3-integrin and alphavbeta5-integrin expression with 18F-fluciclatide for assessment of response to targeted therapy: ready for prime time? J Nucl Med 2011; 52: 335-337.

[80] Battle MR, Goggi JL, Allen L, Barnett J and Morrison MS. Monitoring tumor response to antiangiogenic sunitinib therapy with 18F-fluciclatide, an ^{18}F-labeled alphaVbeta3-integrin and alphaV beta5-integrin imaging agent. J Nucl Med 2011; 52: 424-430.

[81] Sharma R, Kallur KG, Ryu JS, Parameswaran RV, Lindman H, Avril N, Gleeson FV, Lee JD, Lee KH, O'Doherty MJ, Groves AM, Miller MP, Somer EJ, Coombes CR and Aboagye EO. Multicenter Reproducibility of [18F]-fluciclatide PET imaging in subjects with solid tumors. J Nucl Med 2015; 56: 1855-1861.

[82] Wang L, Shi J, Kim YS, Zhai S, Jia B, Zhao H, Liu Z, Wang F, Chen X and Liu S. Improving tumor-targeting capability and pharmacokinetics of ^{99m}Tc-labeled cyclic RGD dimers with PEG$_4$ linkers. Mol Pharm 2009; 6: 231-245.

[83] Jia B, Liu Z, Zhu Z, Shi J, Jin X, Zhao H, Li F, Liu S and Wang F. Blood clearance kinetics, biodistribution, and radiation dosimetry of a kit-formulated integrin alphavbeta3-selective radiotracer [99m]Tc-3PRGD 2 in non-human primates. Mol Imaging Biol 2011; 13: 730-736.

[84] Yoon HJ, Kang KW, Chun IK, Cho N, Im SA, Jeong S, Lee S, Jung KC, Lee YS, Jeong JM, Lee DS, Chung JK and Moon WK. Correlation of breast cancer subtypes, based on estrogen receptor, progesterone receptor, and HER2, with functional imaging parameters from ^{68}Ga-RGD PET/CT and ^{18}F-FDG PET/CT. Eur J Nucl Med Mol Imaging 2014; 41: 1534-1543.

[85] Kim YI, Yoon HJ, Paeng JC, Cheon GJ, Lee DS, Chung JK, Kim EE, Moon WK and Kang KW. Prognostic value of ^{68}Ga-NOTA-RGD PET/CT for predicting disease-free survival for patients with breast cancer undergoing neoadjuvant chemotherapy and surgery: a comparison study with dynamic contrast enhanced MRI. Clin Nucl Med 2016; 41: 614-620.

[86] Zheng K, Liang N, Zhang J, Lang L, Zhang W, Li S, Zhao J, Niu G, Li F, Zhu Z and Chen X. ^{68}Ga-NOTA-PRGD2 PET/CT for integrin imaging in patients with lung cancer. J Nucl Med 2015; 56: 1823-1827.

[87] Haubner R, Finkenstedt A, Stegmayr A, Rangger C, Decristoforo C, Zoller H and Virgolini IJ. [^{68}Ga]NODAGA-RGD-Metabolic stability, biodistribution, and dosimetry data from patients with hepatocellular carcinoma and liver cirrhosis. Eur J Nucl Med Mol Imaging 2016; 43: 2005-2013.

[88] Lopez-Rodriguez V, Galindo-Sarco C, Garcia-Perez FO, Ferro-Flores G, Arrieta O and Avila-Rodriguez MA. PET-based human dosimetry of the dimeric alphavbeta3 integrin ligand ^{68}Ga-DOTA-E-[c(RGDfK)]2, a potential tracer for imaging tumor angiogenesis. J Nucl Med 2016; 57: 404-409.

[89] Edwards D, Jones P, Haramis H, Battle M, Lear R, Barnett DJ, Edwards C, Crawford H, Black A and Godden V. ^{99m}Tc-NC100692--a tracer for imaging vitronectin receptors associated with angiogenesis: a preclinical investigation. Nucl Med Biol 2008; 35: 365-375.

[90] Hua J, Dobrucki LW, Sadeghi MM, Zhang J, Bourke BN, Cavaliere P, Song J, Chow C, Jahanshad N, van Royen N, Buschmann I, Madri JA, Mendizabal M and Sinusas AJ. Noninvasive imaging of angiogenesis with a ^{99m}Tc-labeled peptide targeted at alphavbeta3 integrin after murine hindlimb ischemia. Circulation 2005; 111: 3255-3260.